Heliyon 9 (2023) e17861

Contents lists available at ScienceDirect

Heliyon

journal homepage: www.cell.com/heliyon

Experimental evaluation of the effect of ozone treatment on the oxidation and removal of dry soot deposits of the exhaust gas recirculation system

Jesús Vence, Concepción Paz *, Eduardo Suárez, Adrián Cabarcos, Marcos Conde-Fontenla

CINTECX, Universidade de Vigo, Campus Universitario Lagoas-Marcosende, 36310, Vigo, Spain

ARTICLE INFO

Keywords:
Soot
Ozone treatment
Oxidation
Removal
EGR

ABSTRACT

The integration of alternative energy sources as a replacement for fossil fuels across various industrial sectors, including power generation, emergency systems, or marine applications, is uncertain. As a result, the utilization of traditional fuels is not anticipated to be fully phased out in the near future. To address this, new technologies, such as those that employ oxidising atmospheres, have been explored as a means to enhance the pollution control capabilities of existing technologies, as the Exhaust Gas Recirculation (EGR) system. In this regard, the present study has assessed the efficacy of ozone atmosphere exposure in mitigating the formation of undesired fouling deposits within the system, with the aim of facilitating more efficient operation of EGR devices and extending their service life. To this end, dry soot samples have been exposed to various ozone atmospheres at different temperatures and ozone concentrations through the utilization of an experimental test bench. The oxidation potential of these atmospheres has been evaluated through the analysis of the deposit mass loss. Likewise, confocal microscopy techniques have been employed to obtain the 3D topography of the fouling samples before and after the ozone treatment, allowing the assessment of the deposit thickness reduction, as well as the surface roughness variation. Additionally, thermogravimetric analysis has been conducted to examine the effects of the oxidation processes on fouling samples composition. The findings of this study have revealed that ozone atmospheres have been effective in reducing deposit mass at ozone treatment temperatures above 100 °C. The reduction in mass has reached 78.5% and 91.8% with treatment temperature of 140 °C with ozone concentrations of 30 gO_3/m^3 and 50 gO_3/m^3, respectively. It has also been established that treatment conditions with ozone concentrations of 30 gO_3/m^3 and 50 gO_3/m^3 are effective in reducing the thickness of deposits even at intermediate treatment temperatures, resulting in a thickness reduction of 78.6% and 81.1% at 80 °C, respectively. Additionally, it has been observed that the ozone exposure leads to the increase in the proportion of volatile material within the deposit.

1. Introduction

In order to achieve the main goals of the Paris Agreement, the actual global tendency to reduce greenhouse gas (GHG) emissions,

* Corresponding author.
E-mail address: cpaz@uvigo.es (C. Paz).

https://doi.org/10.1016/j.heliyon.2023.e17861
Received 23 February 2023; Received in revised form 29 June 2023; Accepted 29 June 2023
Available online 7 July 2023

both in transportation and industrial sectors, has prompted the development of greener technologies and the use of fuels with smaller carbon footprint [1]. The movement toward a higher degree of electrification of powertrains, the employment of fuels with higher levels of renewable biofuel content, the use of hydrogen blending fuels or the adoption of hybrid and dual operating modes, are the main strategies that are being pursued to the transition to a low-carbon scenario [2,3]. Under these circumstances, although internal combustion engines (ICEs) are currently facing increasing scrutiny due to concern about pollutant emissions and climate change, they are likely to continue to play a significant role in the forthcoming years in diverse industrial sectors, like off-road applications, marine sector, mining tools, emergency systems or industrial vehicles as excavation, construction and agricultural machinery, combined with synthetic or biofuels [4]. Consequently, the new-age internal engine technologies are expected to increase in the near future as a means of reducing pollutant emissions while maintaining the high performance and convenience of traditional engines [5–7].

To mitigate the exhaust emissions produced by ICEs, one promising approach that has garnered increasing attention in recent years is the use of non-thermal plasma (NTP) [8–11]. This technique involves the employment of plasma, which is produced by the discharge ionization of gas under low temperature conditions, to the generation of highly reactive gas species, as ozone (O_3), and also electrons, ions, and reactive free radicals [12,13]. These reactive substances can promote complex chemical reactions that are able to oxidize a wide range of pollutants under normal operating conditions, including hydrocarbons (HC), nitrogen oxides (NO_x) and particulate matter (PM), breaking them down into less harmful compounds [14,15]. The benefits of using oxidant species to promote the engines exhaust emissions abatement were investigated in several studies and, depending on the strategy employed, they can be classified in three groups: systems that are based on the injection of ozone into the engine combustion chamber, methods focused on the generation or addition of plasma-ozone to the exhaust gas flow, and techniques designed to the regeneration of pollution control devices through ozone exposure.

The first category includes the studies that, based on NTP techniques, generate ozone to be injected into the cylinders of the engine, with the aim of carry out less pollutant combustion processes, such as those conducted by Insani et al. [16], Alipour et al. [17] or Gong et al. [18]. Insani et al. [16] explored the effectiveness of ozone when was added to the air supplied in the combustion chamber of a diesel engine. Employing a Dielectric Barrier Discharge (DBD) method they generated different ozone concentrations and evaluated the performance of the engine under various operating conditions, obtaining that the addition of ozone increased the cylinder pressure and improved the combustion process, leading to the reduction of the pollutant load of the exhaust flow. Alipour et al. [17] analysed the potential of ozone for combustion improvement in a compressed-natural-gas/diesel engine, determining the energy and exergy balance for different operating regimes. Their results suggested that the increased ozone amount augmented the energy and exergy efficiency of the engine and that ozone usage led to the emissions reduction of CO and HC, although at the expense of the increased NO_x emissions. Gong et al. [18] evaluated the effect of ozone addition on combustion processes of a direct injection spark ignition methanol engine during cold start and steady-state conditions, reporting that ozone can increase the formation and oxidation of formaldehyde, especially during the cold start phase of the engine.

The second category encompasses the studies of Madhukar et al. [19], Fan et al. [20], Gao et al. [21,22], Wang et al. [23] or Babaie et al. [24], that analysed both the strategy in which the exhaust gas flowed through the NTP reactor and it got exposed to the electrical discharge plasma–known as direct plasma processing–and the approach of injecting plasma-ozone inside the exhaust line–known as indirect plasma processing–. It was proven that indirect plasma processing had a good performance in converting NO_x and resulted in a more HC reduction and conversion as compared to that with direct plasma method. In addition, it was reported that plasma employed in these techniques owned strong oxidising properties that led to the partial oxidation of PM produced by diesel engines, decreasing the primary diameter of particles, reducing the proportion of its volatile material, and causing the transformation of the core-shell like structure of the particles into densely arranged fringe bands.

The use of pollution control devices, as Diesel Particulate Filters (DPF) or Exhaust Gas Recirculation (EGR) systems, have been effective technologies in helping ICEs meet the new rigorous pollution standards and reduce their impact on the air quality [25,26]. The NTP technique has also been employed to regenerate these antipollution systems and the third category is composed of the studies of Shi et al. [27–29], Pu et al. [30] or Kuwahara et al. [31], that evaluated the effectiveness of this technique on the oxidation and removal of the particulate matter deposited in DPFs, and those carried out by Li et al. [32], Shi et al. [33] or Chen et al. [34], that assessed the suitability of NTP to the regeneration of EGR coolers. Through the evaluation of different operating conditions, these studies indicated that ozone exposure produced the decomposition of the fouling layer, however the oxidative and removal potential of the ozone injection process can vary depending on the specific conditions under which the deposits were generated. Therefore, further research is needed to fully understand the potential benefits and limitations of this technique to define a viable and effective cleaning strategy.

In order to expand upon the knowledge of the effectiveness of NTP in the oxidation and removal process of dry deposits of the EGR system and with the aim of define the most favourable operating parameters, this study analyses the effectiveness of this technique under different ozone exposition scenarios. Employing an oxygen-fed NTP technology, dry soot probes–which were generated reproducing the dry soot deposit of the EGR system–were exposed to ozone atmospheres with different temperatures and ozone concentrations. The reduction of the mass of the soot samples was evaluated and the 3D topography of the fouling layer was captured before and after the oxidative process employing a non-destructive optical technique, allowing to determine the deposit thickness variation. An evaluation of the mean profile of the deposit was performed to determine the average roughness variation induced by the ozone treatment. In addition, the influence of the ozone exposure on the fouling layer composition was evaluated by thermogravimetric analysis (TGA), identifying the proportion of the volatile fraction and the elemental carbon affected by the oxidation process.

2. Materials and methods

The main steps followed in this study are presented in the flowchart of Fig. 1. Firstly, the soot sample was generated in an experimental test bench that reproduces the exhaust gas flow generated by an internal combustion engine. Subsequently, the soot sample was analysed by measuring its mass, performing a thermogravimetric analysis of the fouling, and measuring the 3D topography of the deposit. Next, the soot sample was placed in the ozone exposure test bench, and subsequently subjected to the ozone exposure test. Finally, the sample was removed from the reactor chamber and was analysed again. The following sections present a detailed description of the materials and the methodology employed in each of these steps.

3. Materials

To generate the soot samples, propane gas and nitrogen gas were used as raw materials, and their respective characteristics are listed in Table 1.

3.1. Generation of the EGR fouling samples

The fouling samples employed in this study were generated on an experimental layout that was designed to reproduce deposits caused by the accumulation of dry soot particulate matter, which was described in previous studies [35–37]. To avoid interferences between different parameters of the exhaust gas that can be generated by real ICEs, this experimental test bench is based on a Minicast 5203C soot generator that employs propane and nitrogen as raw materials to produce exhaust flows with strictly controlled conditions.

Given the low cohesiveness of the fouling layer and its susceptibility to be damage, a compact heat exchanger comprising of two modular flat plates was utilised to generate the soot samples, thus enabling a thorough examination of the fouling layer without compromising the integrity of the deposit. As shown in Fig. 2-a, this heat exchanger features a single-pass rectangular channel design, with an inlet hydraulic diameter of 13.79 mm, and comprises of two aluminium flat plates arranged in a symmetrical offset configuration, through which the exhaust gases pass. Each of these plates possess three circular sockets, in which the three 14.5 mm diameter test probes are situated (Fig. 2-b). As shown in Fig. 2-c, once the fouling process is completed and fouling layer is formed on the heat exchanger surface, these probes can be detached from the plate without altering the deposit, resulting in the soot samples employed in this study.

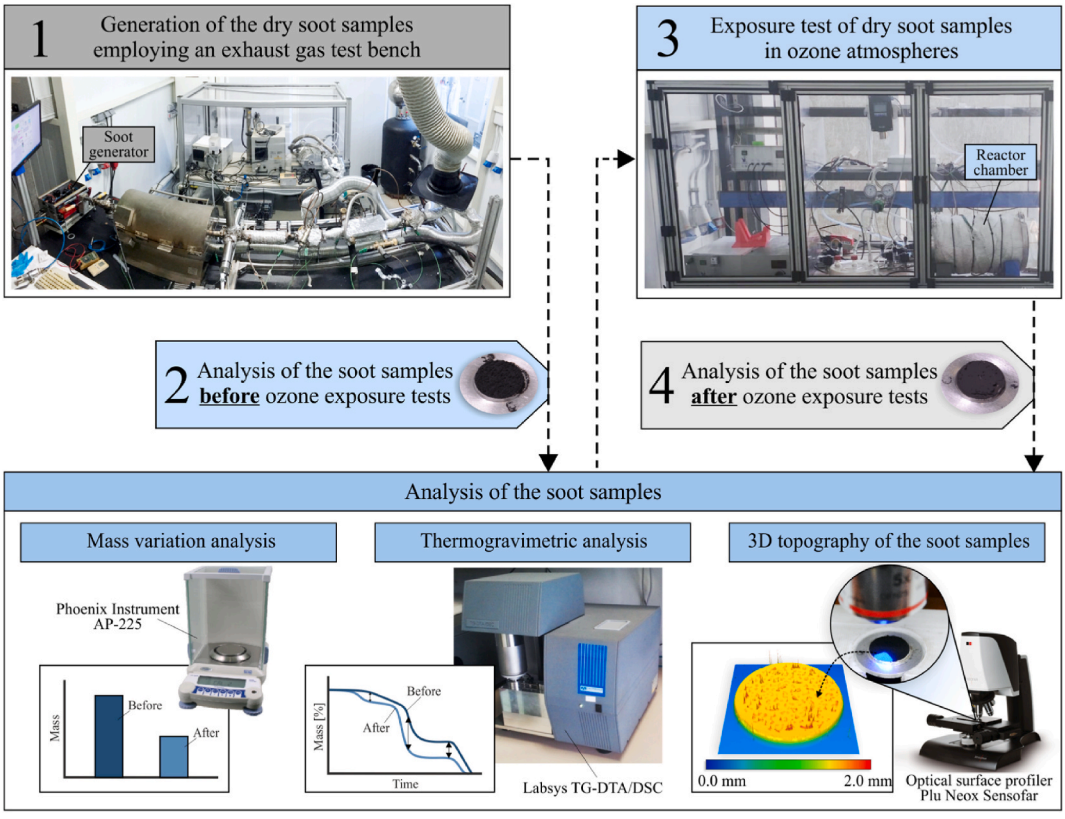

Fig. 1. Flowchart of the experimental methodology followed in this study.

Table 1
Raw materials for the generation of the dry soot samples.

Raw material	Characteristics		Supplier
	Purity percentage	Impurities	
Propane (C_3H_8) gas	99.5%	C_3H_6 < 1000 ppm N_2 < 800 ppm O_2 < 200 ppm H_2 < 100 ppm CO_2 < 50 ppm H_2O < 50 ppm	Air Liquide (Madrid, Spain)
Nitrogen (N_2) gas	99.9%	$H_2O \leq 3$ ppm O2 ≤ 2 ppm CnHm ≤0.5 ppm	Air Liquide (Madrid, Spain)

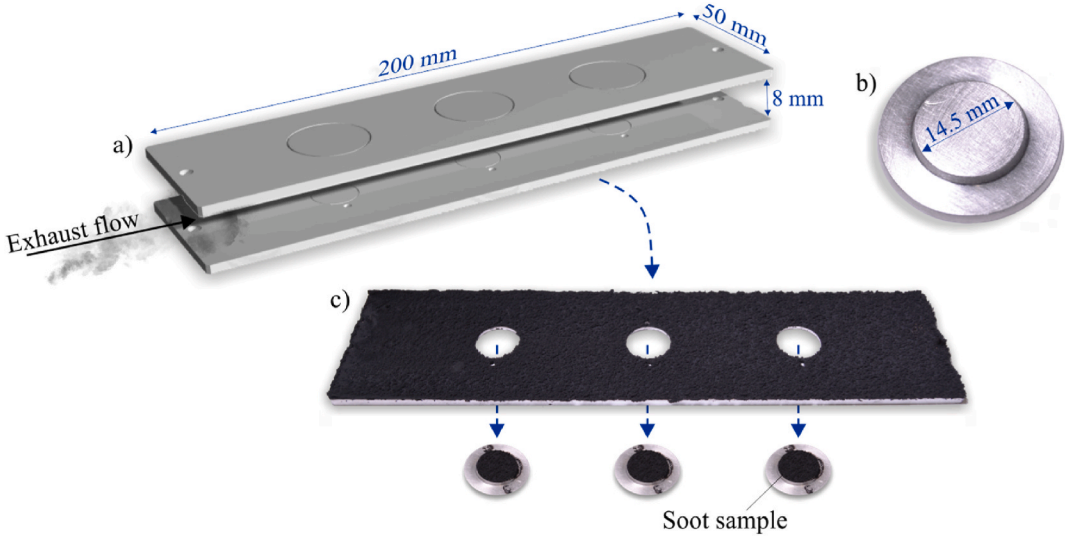

Fig. 2. Schematic of the test section: (a) arrangement of the plates and probes of the heat exchanger, (b) photograph of a probe and (c) photograph of a fouled plate and its three soot samples.

To obtain representative samples of fouling produced within the EGR system, 8 h fouling test periods were executed, by selecting a mass flow rate of 8 kg/h in the exhaust stream and maintaining the gas temperature of 200 °C to ensure the generation of dry soot deposits [38]. The particulate matter of the exhaust flow presented a lognormal distribution with particle diameters ranging from 15 to

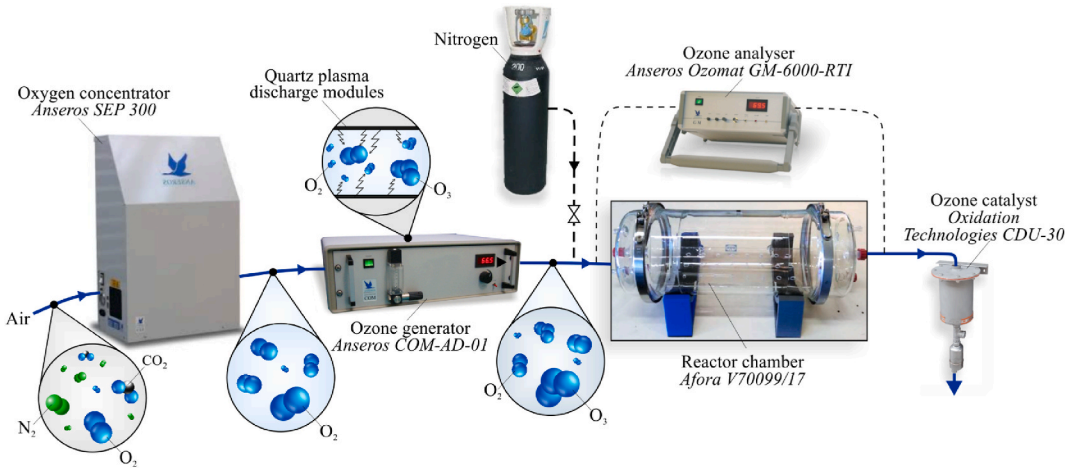

Fig. 3. Scheme of the ozonation tests bench.

615 nm and a total mass concentration of 840 μg/m^3. The heat exchanger was operated with a fixed inlet coolant temperature of 25 °C and a coolant volume flow rate of 2500 L/h, which is sufficient to prevent local coolant boiling within this system.

3.2. Ozone exposure test bench

The experimental test bench used to expose soot samples to different ozone atmospheres is shown in Fig. 3, where the main components of the set-up are depicted. This set-up is described in detail in a previous study [39].

The initial component of this ozone exposure test bench is the Anseros SEP 300. This oxygen concentrator generates an oxygen flow (up to 600 NL O_2/h) from ambient air by utilizing chemical sieves that selectively absorb nitrogen molecules while preserving oxygen molecules, resulting in a maximum purity of 95% ± 5%. This oxygen-rich gas flow then enters the Anseros COM-AD-01 ozone generator. Within this device, the stable oxygen molecules obtained from the concentrator are dissociated into oxygen radicals via the utilization of quartz plasma discharge modules. These radicals are subsequently able to react and form ozone. This component produces ozone flows with concentrations ranging from 0.1 to 190 gO_3/Nm^3.

The gas flow produced at the output of this generator subsequently enters a borosilicate reactor chamber (Afora V70099/17), which has a volume of 0.015 m^3. The fouling samples under examination are situated within this chamber, where the chemical reactions between the ozone and the soot samples occur. To manage the temperature inside the chamber, four electrical heating blankets (Watlow Silicone Rubber Heaters, 0.8 W/cm^2) are affixed on the exterior surface of this reactor. This electrical heating system, whose total power is 1.8 kW, enables to heat the reactor chamber atmosphere up to 180 °C.

The ozone concentration withing the reactor chamber is monitored using the Anseros Ozomat GM-6000-RTI analyser, that assess the light absorption generated by a 253.7 nm wavelength ultraviolet lamp, and which has an operational measurement range between 1 and 200 gO_3/Nm^3. The temperature inside the reactor chamber is monitored using RS Pro 611–8264 class B PT100 sensors. Additionally, a pressure relief valve is implemented to ensure that the maximum allowable absolute pressure of 1.5 bar inside this component is not exceeded.

To ensure secure operational conditions and minimise the operator exposure to high ozone concentrations during the reactor manipulation procedures, an intake pipe situated between the ozone generator and the reactor camber facilitates the supply of a nitrogen flow to the interior of the experimental facility, enabling the evacuation of any remaining ozone from the test bench. Furthermore, in consideration of the toxic nature of ozone, the CDU-30 catalyst unit is positioned at the outlet of the experimental line, ensuring the decomposition of ozone into oxygen.

The entire setup is enclosed within a cabinet equipped with a gas extraction system. The ozone concentration within this enclosure is continuously monitored by a GFG EC28 detector (with a measurement range of 0–1 ppm) to detect potential leaks that may pose an operational hazard.

3.3. Ozone exposure test procedure

The ozone exposure test method began with the warmup period of the oxygen concentrator and the ozone generator. During this phase, the 60 L/h gas flow generated by these devices was routed through a bypass, preventing its entry into the reactor until the required test conditions were attained. Simultaneously, during this warmup phase, the temperature within the reaction chamber was adjusted via the utilization of the electrical heating blankets.

Subsequently, the sample was inserted into the reactor, which was then sealed to initiate the ozone exposition phase. After achieving the required operating conditions, the ozone exposure phase began, and the generated gas flow was directed into the reactor chamber. In order to accurately evaluate the effect of ozone oxidation on the fouling sample and draw precise conclusions, the sample was exposed to the ozone atmosphere for 1 h. During this phase, the temperature and ozone concentration within the reactor chamber were continuously monitored.

Upon completion of the ozone exposure phase, the injection of ozone into the reactor chamber was halted. To eliminate any remaining ozone from the reactor chamber prior to opening it, a nitrogen flush was performed for a duration of 30 min. Subsequently, the reactor chamber was opened, and the fouling sample was extracted from the interior.

In order to define the convenient cleaning strategy and the appropriate operating range to achieve effective reduction of fouling in the EGR system, tests were conducted with different ozone atmospheres. Therefore, the effectiveness of this technique was evaluated for four ozone concentrations: 0, 10, 30 and 50 gO_3/m^3. Additionally, as different operating conditions in the EGR system can expose the fouling to various temperatures, tests were performed by varying the temperature between 40°C–which can be reached during the cold start phase of the engine [40]–, and 140°C–that can be reached during normal operation of the device. A total of 38 ozone exposure tests were conducted taking into consideration the specified ranges.

3.4. Analysis of the mass and topography of the fouling samples

To conduct the analysis of mass reduction of the soot sample caused by the oxidation induced by the ozone atmosphere, the soot sample was weighed before and after the ozone exposure test using the Phoenix Instrument AP-225 precision electronic balance (reproducibility ≤0.1 mg, linearity ±0.3 mg).

Another interesting variable to evaluate the effectiveness of this technique is the analysis of the thickness reduction of the deposit. Therefore, in this study, measurements of the thickness of the fouling samples were taken before and after being subjected to the ozone treatment.

The three-dimensional (3D) topography of the fouling samples was captured using the optical surface profiler PLu Neox Sensofar (spatial resolution of 0.01 nm, linearity of 0.03%) configured in the confocal microscopy mode. Thus, following a protocol proposed in previous studies [41,42], a 5 × optical zoom lens was utilised to obtain the spatial coordinates of the points on the sample surface via non-contact methods, ensuring that the fouling deposit remained undamaged during the measurement process.

The thickness of the fouling samples prior to and following the ozone treatment was determined by measuring the surface of the sample before (Fig. 4-a) and after the ozone test (Fig. 4-d), as well as that of the clean probe (Fig. 4-g). To obtain the complete 3D map, the topographies were processed by using Gwyddion [43] analysis software (Fig. 4-b, -e, -h). An algorithm was developed to calculate the average profile of the upper surface of the deposit considering the entire samples area (Fig. 4-c, -f, -i). This algorithm, that was executed in Matlab, employed different functions based on Hough Transform method to compute and contrast the 3D topographies [44]. By comparing the profiles of the treated and the untreated sample to the clean probe, this algorithm enabled the calculation of the sample thickness variation.

Due to the texture of fouling plays a crucial role in the removal mechanisms of particulate matter from the deposit [36], the roughness of the fouling layer was analysed before and after the ozone treatment. The roughness of the deposit, from the average thickness profile, was evaluated employing the roughness average (R_a) parameter, which computes the arithmetic deviation of the profile from the mean value, as equation (1) depicts:

$$R_a = \frac{1}{N}\sum_{i=1}^{N}|r_i| \tag{1}$$

where N represents the number of points of the average profile and r_i is the distance from the mean line to the i_{th} data point.

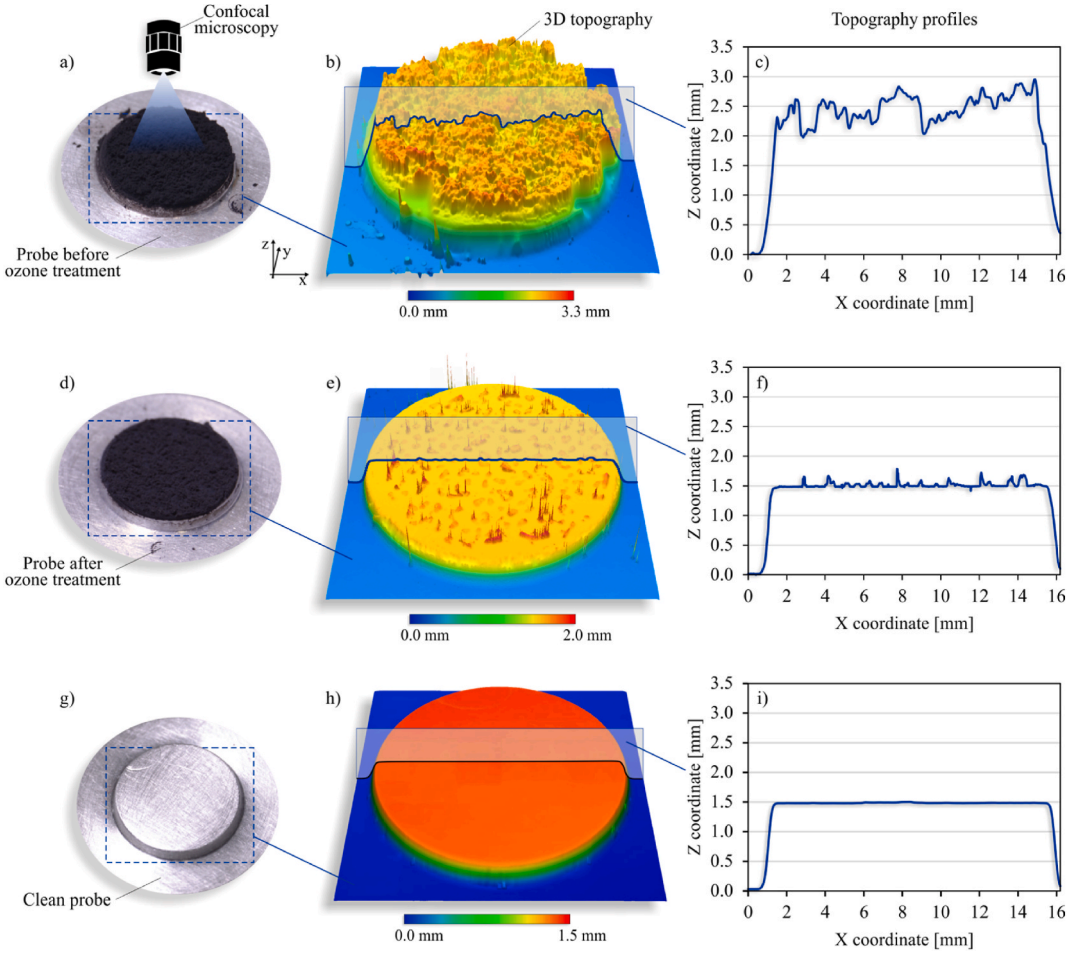

Fig. 4. Schematics of the methodology of topography measurements: (a), (d) and (g) sections of the probes that were captured employing confocal microscopy, (b), (e) and (h) 3D topography of the samples and (c), (f) and (i) profiles obtained from the 3D topography.

3.5. Thermogravimetric analysis

In order to identify the impact of the ozone treatment on the composition ratio of the volatile compounds and soot fraction of the fouling samples, thermogravimetric analysis (TGA) was conducted. The mass composition ratio of the different fouling components was analysed before and after the ozone treatment following a methodology similar to that employed in previous studies [45–47]. Table 2 summarises the thermal protocol of the thermogravimetric tests and the representative compound of each temperature range. The volatile fraction was divided into water, light HC–HC with low number of C atoms and high volatility–and heavy HC–HC with high number of C atoms and low volatility–. Under the nitrogen atmosphere, water fraction was defined by mass loss under the temperature ranging from room temperature to 120 °C. Light HC was estimated by the weight of samples from 120 °C to 350 °C and heavy HC was obtained by the weight variation between 350 °C and 750 °C. After changing atmosphere from nitrogen to oxygen, keeping the temperature constant, elemental carbon and ash were identified.

4. Reaction mechanisms of fouling reduction based on ozone exposure

Inside the ozone generator, the dielectric barrier discharge process produces that oxygen molecules dissociate in oxygen atoms, causing that molecules of oxygen form oxygen atoms and ozone molecules, as shown in the reactions 2–4 [48]:

$$O_2 + e \rightarrow 2\,O\left(O_2^*\right) \tag{2}$$

$$O_2 + O \rightarrow O_3 \tag{3}$$

$$O_2^* + O_2 \rightarrow O_3 + O \tag{4}$$

In this manner, the gas stream that enters the reactor is composed of oxygen, ozone, and oxygen atoms, of which the latter two species present the higher oxidative potential.

The fouling layers generated inside the EGR system are mainly composed of dry soot–elemental carbon–, adsorbed HC–the soluble organic fraction (SOF)–an a small amount of inorganic salt [49,50]. Both the dry fraction and adsorbed HC can be oxidised by the reactive species present in the plasma flow. The heterogeneous mechanism that takes place on the deposit surface, involving the interaction between highly reactive species and the fouling layer, is summarized in the following chemical reactions [30,31,51]:

$$O + HC \rightarrow RO_2, RO, OH \tag{5}$$

$$O_3 + SOF \rightarrow CO(CO_2) + O_2 + H_2O \tag{6}$$

$$C + O \rightarrow CO \tag{7}$$

$$C + 2O \rightarrow CO_2 \tag{8}$$

$$C + O_3 \rightarrow CO + O_2 \tag{9}$$

$$C + 2O_3 \rightarrow CO_2 + 2O_2 \tag{10}$$

Equation (5) represents the oxidation of HC by oxygen to form different oxygen radicals, as peroxyl radicals (RO_2), alkoxyl radicals (RO) or hydroxyl radicals (OH) [52]. RO_2 radicals are formed when oxygen reacts with HC to create a reactive intermediate, which then reacts with more oxygen to produce RO_2. RO radicals are produced when hydrogen atoms from hydrocarbons is abstracted by oxygen, that becomes a RO radical. OH radicals are produced via a secondary reaction between RO_2 and another HC molecule.

Equation (6) shows the chemical reactions between the soluble organic fraction and ozone.

Equations (7)–(10) represent the oxidative reactions of the dry soot compounds. As these chemical processes reveal, CO and CO_2 gases are the prevalent compounds that are produced as a result of these reactions. Given the degradation process of soot deposits employing ozone atmospheres will result in the production of gaseous pollutants, such as CO and CO_2, subsequent analyses will need to be carried out to evaluate the net production of pollutants. This analysis should focus on the combustion process of modern internal engines, taking into account both the effectiveness of the proposed technique in improving the performance of EGR system to reduce

Table 2
Experimental protocol of the thermogravimetric tests and representative compound of each temperature range.

Step	Atmosphere conditions	Representative compound
1	N_2 atmosphere, from room temperature to 120 °C, heating rate 10 °C/min	Water
2	N_2 atmosphere, 120 °C, isothermal for 10 min	
3	N_2 atmosphere, from 120° to 350 °C, heating rate 10 °C/min	Light HC
4	N_2 atmosphere, 350 °C, isothermal for 10 min	
5	N_2 atmosphere, from 350° to 750 °C, heating rate 10 °C/min	Heavy HC
6	N_2 atmosphere, 750 °C, isothermal for 10 min	
7	N_2 + O_2 atmosphere, 750 °C, isothermal for 30 min	Elemental carbon + ash

NO_x emissions and the products resulting from its application.

5. Results and discussions

To provide the degree of uncertainties of the results and to ensure the reliability of the research finding, the tests repeatability was evaluated based on nineteen tests, covering the entire spectrum of ozone concentration and treatment temperatures of this study. As shown in Fig. 5, the comparison of the results of mass reduction achieved in multiple test that were conducted under the same conditions allowed to compute the deviation, which presented an average value of 2.9% and a maximum value of 7%. This maximum value was used as a basis for representing the deviation of the results.

5.1. Effect on the fouling mass

Fig. 6 shows the results of mass reduction occurred after the tests for ozone atmosphere exposure considering different temperatures and the four ozone concentrations.

The analysis of the results in the absence of ozone inside the reactor chamber–0 gO_3/m^3–allowed to determine that the reduction of the mass of the deposit was 4.5% when the reactor temperature was 40 °C. In addition, it was detected that the increase of the temperature led to a greater mass loss, reaching 14.5% when the temperature was 140 °C. With these higher reactor temperatures, the energy of the molecules in the fouling layer also increased, leading to an increment of the rate of evaporation of the volatile compounds, especially water and light HC linked to the particulate matter, which were vaporized and were released into the surrounding atmosphere. The strong bonds between the carbon structure of the deposit made difficult for this low oxidative environment–without ozone–to penetrate and initiate a chemical reaction and, as a result, the soot layer was able to persist, leading to a low mass reduction.

The addition of different concentrations of ozone to the treatment atmospheres allowed to detect two scenarios on the deposit mass variation: a slight increase in the mass of the fouling layer when selecting low temperatures, and a great mass removal effect when high temperatures were considered.

On the one hand, the analysis of the results of the 10 gO_3/m^3 atmosphere allowed to determine that when the environment temperature was lower than 100 °C the mass of the deposit increased, reaching to an increment of 24.4% when the atmosphere temperature was fixed in 40 °C. This effect was more significant when higher ozone concentrations were considered, reaching a mass increase of 27.7% and 35.6% at 40 °C in the cases of 30 gO_3/m^3 and 50 gO_3/m^3, respectively. A feasible interpretation for this phenomenon is the addition of water to the deposit, which could take place once the fouling sample was extracted from the reactor chamber. As various studies reported [53–56], the ozonisation process of soot can change the hygroscopicity of fouling, increasing its water adsorption capacity. This is because, during the ozone treatment, the heterogeneous reaction of ozone and the fouling layer follows a Langmuir-Hinshelwood mechanism [57,58], as shown in Equations (11) and (12), in which the first step is the formation of oxygenated carbon species ($C^*[O]$) on the deposit, and in the second step these compounds react producing carbon oxides [59]:

$$O_3\ (g) + C\ (soot) \rightarrow C^*[O] + O_2(g) \tag{11}$$

$$C^*[O] + C^*[O] \rightarrow CO_2(g) + C(s) \tag{12}$$

The formation of oxygen-containing functional groups onto the surface makes the deposit more polar, increasing its affinity for water. In addition, these reactions induce the reduction of the primary particle size of the particulate matter, revealing more adsorptive sites and augmenting the ability of the fouling layer to interact with water molecules, showing that fouling oxidised by ozone undergoes enhanced hydration [55,60,61]. Thus, notwithstanding the reduction in mass derived from the oxidation reaction induced by

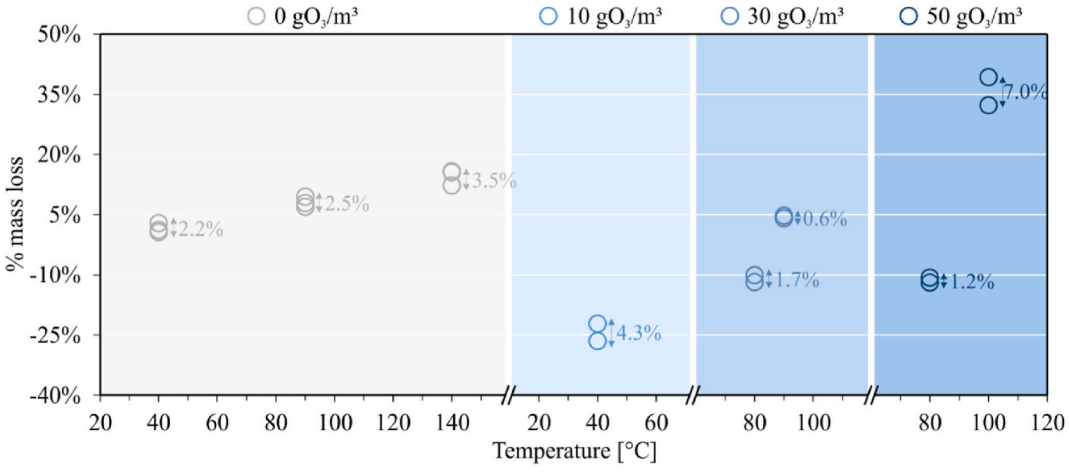

Fig. 5. Repeatability of the measurements for nineteen runs of ozonation treatments.

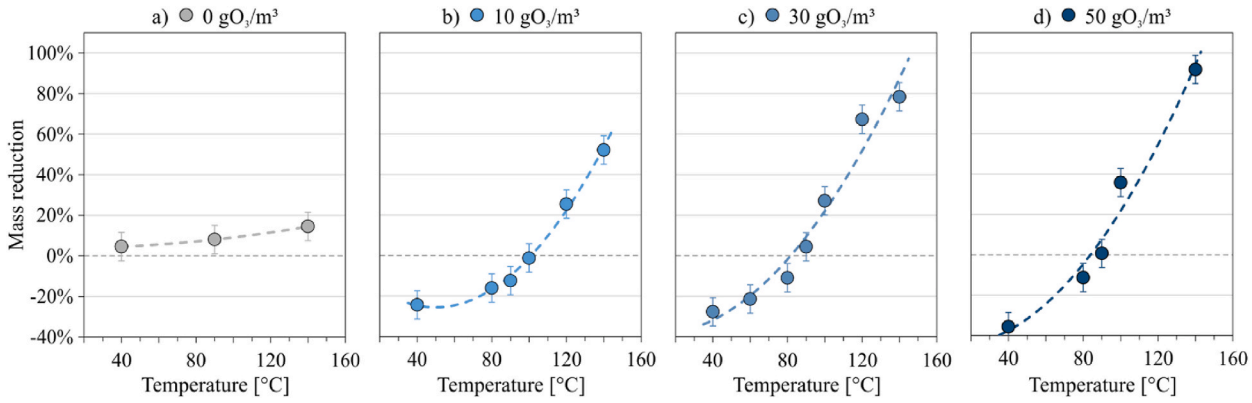

Fig. 6. Results of mass reduction after tests for ozone atmosphere exposure considering different temperatures and ozone concentrations of (a) 0 gO_3/m^3, (b)10 gO_3/m^3, (c) 30 gO_3/m^3 and (d) 50 gO_3/m^3. The error bars represent the maximum deviation detected in the repeatability analysis (±7%).

ozone, the addition of water to the deposit once it was extracted from the reactor chamber resulted in an increase in the final mass balance, most acutely in tests with lower temperature, due to the lower oxidative capacity of these atmospheres. In view of these results, additional research is needed to comprehensively elucidate the mechanism of moisture absorption by the fouling sample. While the results indicate that the ozone treatment of the fouling layer leads to an increase of the deposit mass under the present operating conditions, a more extensive investigation is required to evaluate the oxidative efficacy of ozone treatment and to elucidate how varying humidity levels in the ambient air can affect the removal of fouling. Such research could provide valuable insights into the effectiveness of ozone treatment for the removal of dry soot deposits subsequent to be exposed to varying ambient humidity conditions, as well as inform the development of more efficient and sustainable fouling mitigation strategies.

On the other hand, the assessment of the results of the 10 gO_3/m^3 atmosphere allowed to determine that when the environment temperature was higher than 100 °C, led to the reduction of the mass of the deposit. Moreover, as the graph shows, the higher atmosphere temperature, the greater mass reduction was achieved, reaching a reduction of the 52.1% when the atmosphere temperature was fixed in 140 °C. The comparison with the results of the atmospheres with 30 gO_3/m^3 and 50 gO_3/m^3 revealed that, in agreement with recent studies [27,30], this effect was more marked when higher ozone concentrations were considered. In this manner, the deposit mass reduction achieved with 30 and 50 gO_3/m^3 at 100 °C was 27.1% and 35.8%, respectively, while at 140 °C, the mass loss was 78.5% and 91.8%, respectively. This indicated that, in the three scenarios, the increase of the temperature from 100 °C to 140 °C resulted in a similar increase of the mass reduction, with an average value of 53.6%.

It is important to consider that, as previous studies have mentioned, such as the one carried out by Itoh et al. [62], an increase in temperature is associated with the thermal decomposition of ozone. This indicates that as the temperature increases, ozone degradation to form oxygen increases, resulting in a decrease in ozone concentration. However, for the temperature range selected in this study (40–140 °C), ozone degradation remains below 30%, indicating that this phenomenon does not act as a limiting factor in the oxidation of soot deposits [29].

According to the studies of Lee et al. [59], Friebel et al. [63] or Chughtai et al. [64], the obtained results verified that the oxidation rate between ozone and soot particles increases as reaction temperature rises, and could be as much as 3–5 times higher, as long as the

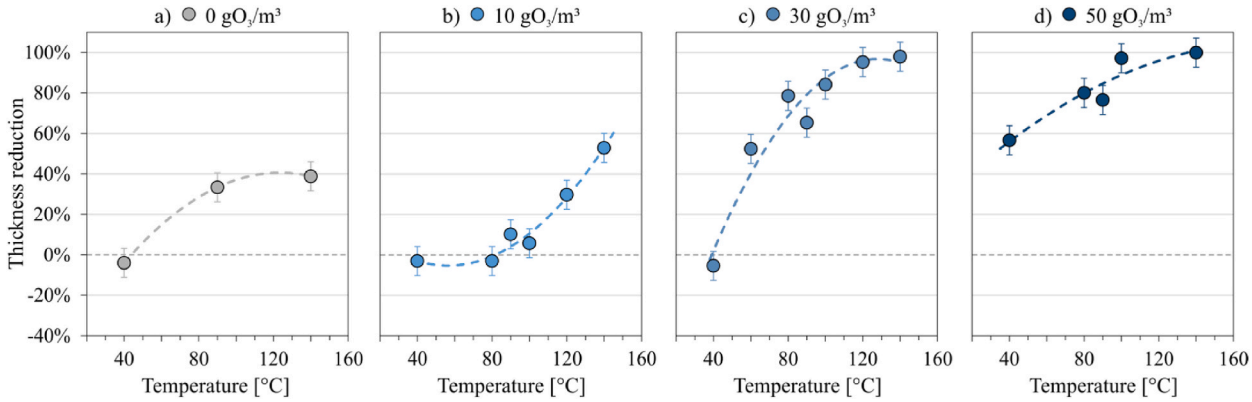

Fig. 7. Results of thickness reduction after tests for ozone atmosphere exposure considering different temperatures and ozone concentrations of (a) 0 gO_3/m^3, (b)10 gO_3/m^3, (c) 30 gO_3/m^3 and (d) 50 gO_3/m^3. The error bars represent the maximum deviation detected in the repeatability analysis (±7%).

thermal decomposition of ozone remains within acceptable levels. The increase of the temperature and ozone concentration encouraged the break of the C═C bonds of the particulate matter of the deposit, and the O atoms were linked to the carbon chain, leading to the formation of C–OH groups, which were gradually oxidised to C═O groups, forming CO_2 and CO [65,66].

The analysis of the results obtained in this section determined that significant reduction in deposit mass can be achieved through ozone treatment at temperatures above 100 °C. Additionally, it was observed that an increase in ozone concentration within the treatment atmosphere resulted in an enhanced oxidation of the deposit, with the highest level of fouling mass reduction observed at a concentration of 50 gO_3/m^3 and a treatment temperature of 140 °C.

5.2. *Effect on the thickness and roughness of the deposit*

Fig. 7 shows the results of thickness reduction occurred after the tests for ozone atmosphere exposure considering the four ozone concentrations and different temperatures.

The analysis of the results in the absence of ozone inside the reactor chamber –0 gO_3/m^3–allowed to detect that, although when the temperature was fixed in 40 °C the thickness of the deposit hardly varied, when the reactor temperature was above 40 °C, the thickness of the fouling sample decreased. The vaporization of a portion of the volatile compounds induced by high treatment temperatures resulted in the reorganization of the internal structure of the deposit, causing the reduction of the thickness of the fouling layer, that reached the 38.8% when the test temperature was fixed in 140 °C.

The study of the results obtained with the atmospheres of 10 gO_3/m^3 enabled the determination that, under the lowest treatment temperatures, a phenomenon similar to that observed in the absence of ozone was detected: the thickness of the samples exhibited minimal deviation. However, at 90 °C it was noticed that the reduction in thickness was notably less than that measured under absence of ozone conditions. This lesser decrease in thickness can potentially be attributed to the preservation of the original structure fouling, induced by the water addition to the deposit. The modification in the hygroscopicity of the fouling sample, resulted from the reaction with ozone and the subsequent increase in water content within the deposit, may have facilitated the maintenance of the original form, thereby preventing the reduction of the deposit thickness. At 90 °C, the loss of volatile material is compensated by the increase in moisture content of the sample, leading the structure of the deposit to remain practically unchanged and, therefore, maintaining the thickness of the soot sample. Nonetheless, it was observed that this phenomenon is only noticeable at treatment temperatures below 120 °C. When treatment temperatures surpassed this threshold, the thickness reduction observed under conditions of 10 gO_3/m^3 ozone concentration was slightly superior to that observed in the ozone-free atmosphere. The enhanced reactivity and oxidative potential of

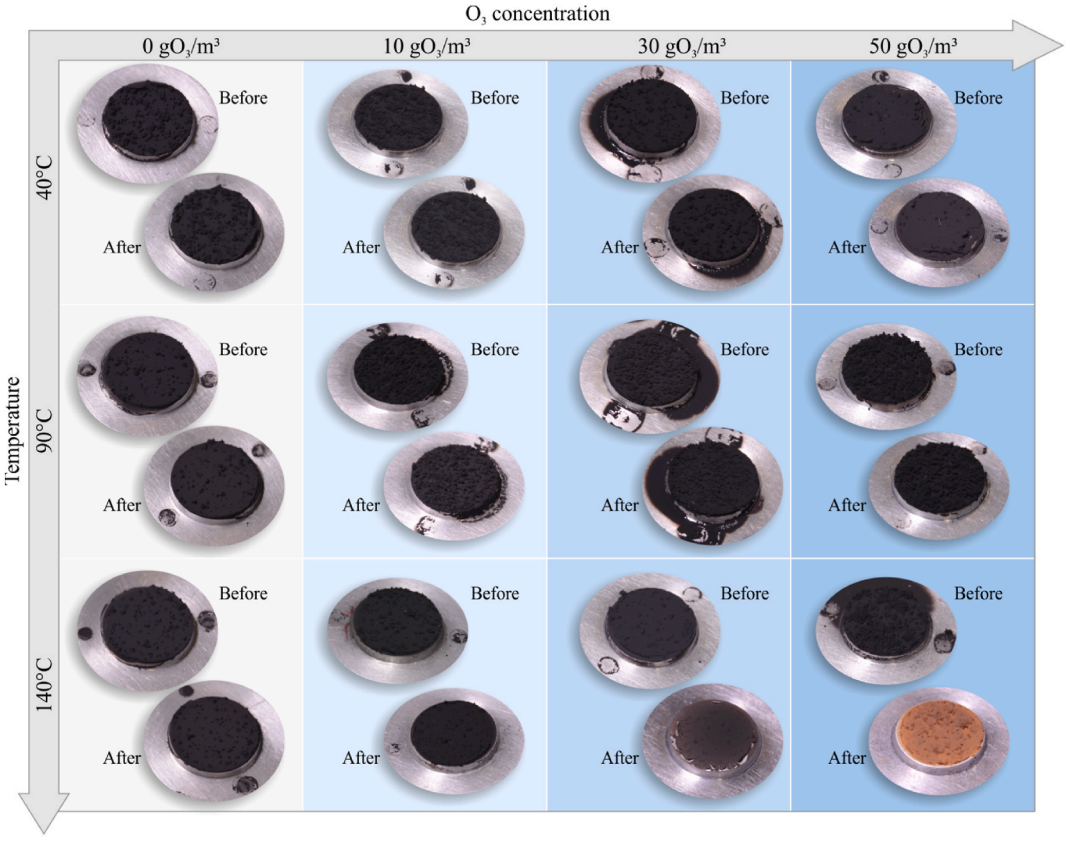

Fig. 8. Photographs of the soot samples before and after the ozone treatment considering different temperatures and ozone concentrations.

the atmosphere at elevated temperatures resulted in an increase in oxidation of the deposit. Therefore, although there may be an increase in the moisture content of the deposit, it was not enough to compensate for the high deposit oxidation that had occurred, which caused significant changes in the internal structure of the deposit and led to a more notable reduction in thickness.

The examination of the results obtained in atmospheres with ozone concentrations of 30 gO_3/m^3 and 50 gO_3/m^3 enabled the confirmation that the rise in ozone concentration in the treatment atmosphere resulted in a substantial decrease in the thickness of the fouling sample. Even at intermediate treatment temperatures, high ozone concentration led to substantial oxidation of the deposits, which translated into a significant decrease in deposit thickness, achieving thickness reductions of 78.6% and 80.1% for treatments at 80 °C, and 84.2% and 97.3% for treatments at 100 °C in atmospheres of 30 gO_3/m^3 and 50 gO_3/m^3, respectively. The employment of higher treatment temperatures revealed an increased significance of this phenomenon. Consistent with the outcomes of the mass reduction analysis, the enhancement of the oxidation ratio resulting from an elevation of the treatment temperature led to a heightened degradation of the internal structure of the deposit, which manifested as a pronounced reduction in sample thickness. This effect was particularly pronounced when the treatment temperature of 140 °C was employed, nearly resulting in complete reduction in both the scenario of 30 gO_3/m^3 and that of 50 gO_3/m^3.

The high oxidative capacity of atmospheres with high ozone concentration and elevated temperature, that resulted in substantial reduction of samples thickness, was also reflected by the modification in the visual aspect of the deposits. As depicted in Fig. 8, in addition to the visible thickness reduction, the deposits treated in these atmospheres also exhibited a change in their appearance and coloration. Starting from a matte black appearance, characteristic of this type of dry soot deposits, the samples underwent a shift in pigmentation to hues of brown, as can be distinctly discerned in the photographs of the sample treated at 140 °C and 50 gO_3/m^3 of Fig. 8.

Fig. 9 shows the results of reduction in the roughness of the deposit after being subjected to the treatment in the ozone atmosphere.

The analysis of the results of the variation in the texture of the deposits revealed that an increase in ozone concentration also produced a significant reduction in the roughness of the deposit. The substantial decrease in thickness observed in deposit treated in atmospheres with high ozone concentrations was accompanied by a reduction in the mean roughness of the deposits, as evident in the cases with concentrations of 30 gO_3/m^3 and 50 gO_3/m^3, with a median R_a decrease of 39.5% and 56.5% respectively. The oxidation of the deposit brought about by the reaction with ozone resulted in homogenization and smoothing of the surface profile of the fouling layer, leading to a less rugged appearance of the deposit sample.

5.3. TG analysis

TGA were performed at least three times for every sample collected, and the average weight loss curves of fouling samples before and after the ozone treatment at 90 °C and 140 °C are presented in Fig. 10a and b, respectively.

The analysis of the results allowed to determine that, during the first steps of the evolution of the furnace temperature, the weight loss curves of the fouling samples that were treated with ozone showed a decrease at a faster rate than the raw samples. This effect, that was observed both in the fouling samples that were exposed to the ozone atmosphere at 90 °C and at 140 °C, revealed an increase of the volatility of the deposit. The reaction of ozone with the surface functional groups of the deposit resulted in the breakdown of C–C bonds, as well as the generation of carbon and oxygen-functional groups, leading to the formation of more volatile species [27,28,67]. Moreover, the presence of OH groups in fouling, due to the more reactive capacity of chemisorbed oxygen, also facilitated its removal from the deposit during oxidation [68,69]. These changes on the configuration of the fouling samples showed that ozone treatment

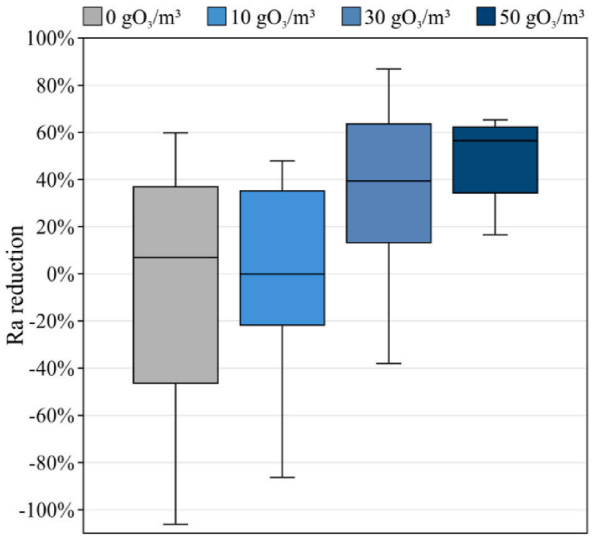

Fig. 9. Distribution of the results of Ra reduction of the soot samples considering different ozone concentrations.

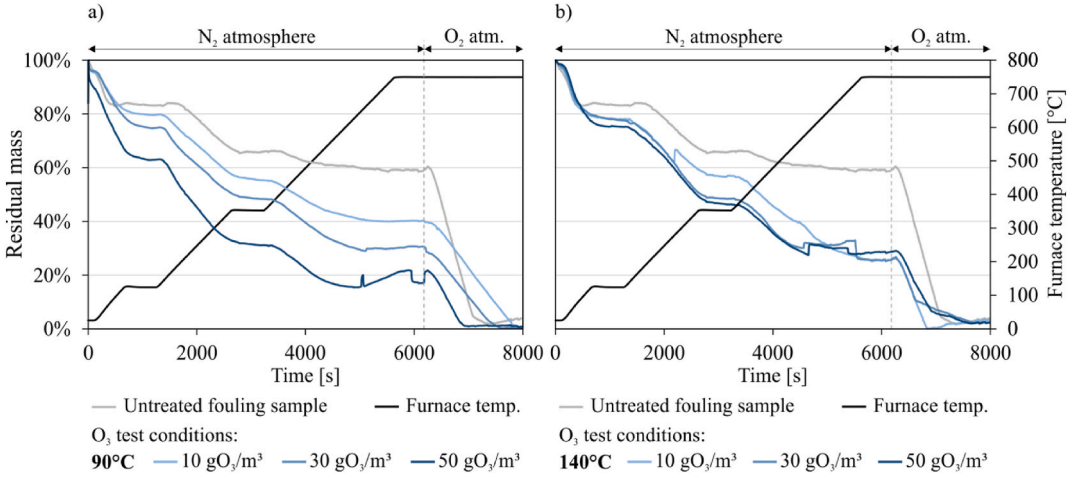

Fig. 10. TG curves of (a) soot samples treated with ozone atmospheres at 90 °C and (b) soot samples treated with ozone atmospheres at 140 °C.

enhanced the volatilization of fouling, making easier the reduction and elimination of the fouling layers mainly composed of PM with carbonaceous structure [11].

The comparison of the weight loss curves obtained with both operating temperatures revealed that in the ozonised fouling at 90 °C the increase of the ozone concentration led to a marked increase of volatile content of fouling, while the samples treated at 140 °C reached a similar stage regardless of the ozone concentration. This effect might have been due to the fact that the fouling samples that were exposed to 140 °C, the high temperature of this atmosphere might have contributed to the vaporization of some of volatile compounds during the ozone treatment, reducing the volatile fraction of the sample. The higher oxidative potential of the ozone atmosphere at 140 °C, particularly with the highest ozone concentrations, led to an increase in the production of volatile species. These volatile species were subsequently vaporized and removed from the soot sample when exposed to a high-temperature atmosphere. This higher mass sample reduction accords with the findings given by the results of sections 4.1 and 4.2, that indicated that at 140 °C the ozonised samples showed higher mass and thickness reduction rates.

Fig. 11 shows the proportion of the different PM components after been treated with ozone atmosphere, where each column represents the mean value, and the error bar depicts the standard deviation of three repeated measurements.

The quantitative analysis of the solid fraction of the fouling samples revealed that the untreated samples generated in this study were primarily composed of soot, with an elemental carbon and ash content of approximately 55%. This determination confirmed the classification of the fouling samples as dry soot fouling [70,71].

The analysis of the solid fraction of the soot samples (carbonaceous compounds and ash) also revealed that using a temperature of 90 °C, an increase in ozone concentration in the treatment atmosphere leaded to a greater reduction in the solid fraction of the sample. However, it was detected that for the use of higher temperatures (140 °C), the increase in ozone concentration in the treatment atmosphere leaded to a similar proportion of the solid fraction. This highlighted that at low treatment temperatures, increasing ozone concentration leaded to an enhancement of the oxidation rate of the solid fraction in the soot samples, resulting in a high reduction of the proportion of carbonaceous compounds. On the contrary, at high treatment temperatures, the reduction of the solid fraction achieved was independent of the ozone concentration used, and the degradation rate on these compounds was similar for these temperatures. At 140 °C the oxidation potential of the ozone atmosphere was high enough to produce a significant reduction in the solid fraction of the soot samples, even at low ozone concentrations, whereas at 90 °C it was necessary to work with higher concentrations to achieve a similar level of degradation. These results are consistent with those obtained in the analyses of variation in sample mass and thickness, which revealed that the increase in treatment atmosphere temperature led to a significant oxidation and, consequently, a greater reduction in thickness and mass of the soot samples.

The analysis of the mass composition ratio of the volatile compounds allowed to determine that the water content of the oxidised samples was higher than that of the untreated samples. Due to the ability of ozone to react with the surface functional groups of fouling and to incorporate oxygen-containing groups onto the deposit, the ozonation reactions increased the affinity of PM for water, enhancing the water-sorbing capacity of the deposit [67,72]. Despite the deposit mass loss, the hygroscopic behaviour of fouling after been exposed to ozone atmospheres led to the increase of the water content ratio as temperature and ozone concentration increased, reaching up to 25% of the mass of the deposit when the 140 °C and 50 gO_3/m^3 conditions were employed.

The analysis of the evolution of the mass ratio of the light HC and heavy HC allowed to detect that the proportion of these two categories increased after been exposed to the ozone atmosphere, as can be seen in the case of 90 °C and 10 gO_3/m^3. As mentioned earlier, the reduction of the carbonaceous compounds led to the increase of the volatile fraction of the samples, particularly the mass ratio of the HC with low volatility. However, it was observed that the use of higher reactive atmospheres, i.e., with higher temperature and higher ozone concentration, resulted in less heavy HC, while at the same time increased the proportion of light HC. The high oxidative potential of these atmospheres resulted in the oxidation-breakdown of the volatile species, that shift from high carbon atom arrangements to low carbon atom arrangements, indicating that this oxidative decomposition process involved the continuous removal

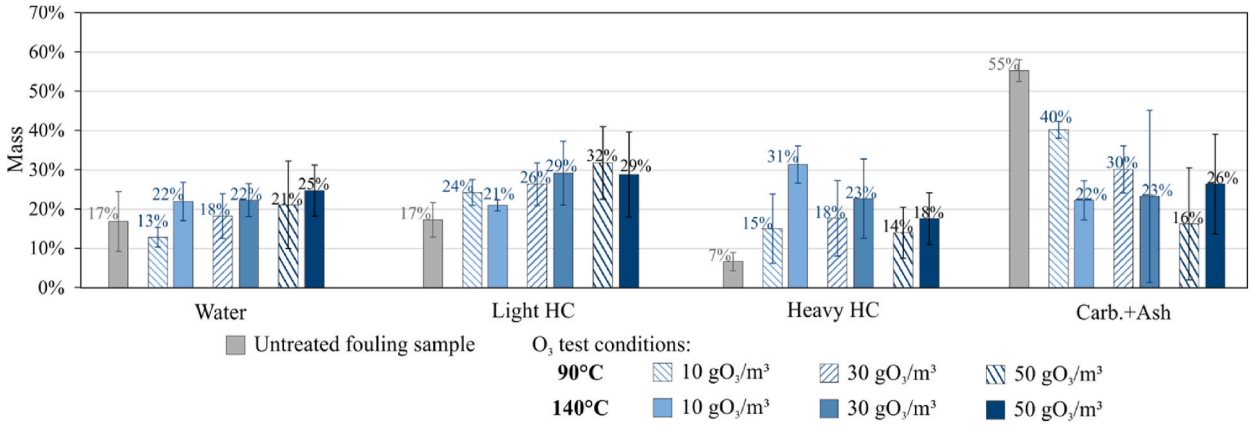

Fig. 11. Mass composition ratio of the volatile compounds and solid fraction of the fouling samples treated with different ozone atmospheres. Columns represent the mean values and error bars represent the standard deviation of three repeated measurements.

of carbon atoms that converted the large molecular structure of the volatile species into smaller molecules [11,28].

6. Conclusions

This study was conducted to investigate the effectiveness of ozone exposure as a method for inducing oxidation and removing dry soot deposits from the EGR system. Dry soot fouling samples were exposed to ozone atmospheres with ozone concentrations ranging from 0 to 50 gO_3/m^3 and temperatures ranging from 40 to 140 °C. The oxidation effectiveness of the different ozone treatment conditions was evaluated through the measurement of the reduction in mass of the soot samples. Moreover, the 3D-topography of the fouling samples was obtained both before and after the exposure process, allowing for the assessment of changes in deposit thickness and surface roughness. Additionally, TGA was performed on the raw samples and the treated deposits, determining the proportion of the volatile fraction and elemental carbon affected by the oxidation process under the varied treatment conditions.

Based on the results obtained, the following conclusions were drawn.

- Significant reduction in deposit mass can be achieved employing ozone atmospheres at temperature above 100 °C.
- The increase in treatment temperature resulted in a higher level of oxidation of the deposit, which was reflected in a greater reduction of the fouling mass. The reduction reached 78.5% and 91.8% when temperatures of 140 °C were used with ozone concentrations of 30 gO_3/m^3 and 50 gO_3/m^3, respectively.
- The thickness of fouling samples experienced a significant reduction when exposed to ozone atmospheres of 30 gO_3/m^3 and 50 gO_3/m^3, even at intermediate treatment temperatures (80–100 °C). Specially, the thickness reduction was 78.6% and 81.1% for treatment conducted at 80 °C in atmospheres of 30 gO_3/m^3 and 50 gO_3/m^3, respectively.
- The application of high ozone concentrations leaded to a substantial decrease in the mean roughness of the deposit surface, as evidenced by a median decrease in R_a of 56.5% when utilizing ozone atmospheres with ozone concentration of 50 gO_3/m^3.
- The TGA tests revealed that treatments in ozone atmospheres increased the proportion of volatile compounds in the fouling samples.

The results obtained from this study provide valuable insights into the behaviour of dry soot deposits when exposed to oxidising atmospheres. These findings will serve as a foundation for the development of future technologies based on this technique, aimed at mitigating the buildup of fouling deposits within the EGR system or other aftertreatment techniques.

Author contribution statement

- Conceived and designed the experiments: Concepción Paz, Jesús Vence.
- Performed the experiments: Eduardo Suárez, Adrián Cabarcos, Marcos Conde-Fontenla.
- Analysed and interpreted the data: Jesús Vence, Concepción Paz, Eduardo Suárez.
- Contributed reagents, materials, analysis tools or data: Adrián Cabarcos, Marcos Conde-Fontenla
- Wrote the paper: Jesús Vence, Concepción Paz, Eduardo Suárez, Adrián Cabarcos, Marcos Conde-Fontenla.

Declaration of competing interest

The authors declare that they have no known competing financial interests or personal relationships that could have appeared to influence the work reported in this paper.

Acknowledgements

Authors are grateful for the financial support from the Spanish Ministry for Science and Innovation through the PDC2021-121778-100 project. Funding for open access charge: Universidade de Vigo/CISUG.

References

[1] P. Miklautsch, M. Woschank, A framework of measures to mitigate greenhouse gas emissions in freight transport: systematic literature review from a Manufacturer's perspective, J. Clean. Prod. 366 (Sep. 2022), 132883, https://doi.org/10.1016/j.jclepro.2022.132883.
[2] I. de Blas, M. Mediavilla, I. Capellán-Pérez, C. Duce, The limits of transport decarbonization under the current growth paradigm, Energy Strategy Rev. 32 (Nov. 2020), 100543, https://doi.org/10.1016/j.esr.2020.100543.
[3] Ö. Andersson, P. Börjesson, The greenhouse gas emissions of an electrified vehicle combined with renewable fuels: life cycle assessment and policy implications, Appl. Energy 289 (May 2021), 116621, https://doi.org/10.1016/j.apenergy.2021.116621.
[4] R.D. Reitz, H. Ogawa, R. Payri, T. Fansler, S. Kokjohn, Y. Moriyoshi, A. Agarwal, D. Arcoumanis, D. Assanis, C. Bae, K. Boulouchos, M. Canakci, S. Curran, I. Denbratt, M. Gavaises, M. Guenthner, C. Hasse, Z. Huang, T. Ishiyama, B. Johansson, T. Johnson, G. Kalghatgi, M. Koike, S. Kong, A. Leipertz, P. Miles, R. Novella, A. Onorati, M. Richter, S. Shuai, D. Siebers, W. Su, M. Trujillo, N. Uchida, B.M. Vaglieco, R. Wagner, H. Zhao, IJER editorial: the future of the internal combustion engine, Int. J. Engine Res. 21 (1) (Sep. 2019) 3–10, https://doi.org/10.1177/1468087419877990.
[5] G. Kalghatgi, Is it really the end of internal combustion engines and petroleum in transport? Appl. Energy 225 (Sep. 2018) 965–974, https://doi.org/10.1016/j.apenergy.2018.05.076.
[6] R. Danielis, M. Scorrano, M. Giansoldati, Decarbonising transport in Europe: trends, goals, policies and passenger car scenarios, Res. Transport. Econ. 91 (Mar. 2022), 101068, https://doi.org/10.1016/j.retrec.2021.101068.
[7] H. Ababneh, B.H. Hameed, Electrofuels as emerging new green alternative fuel: a review of recent literature, Energy Convers. Manag. 254 (Feb. 2022), 115213, https://doi.org/10.1016/j.enconman.2022.115213.
[8] Z. Han, T. Zou, J. Wang, J. Dong, Y. Deng, X. Pan, A novel method for simultaneous removal of NO and SO2 from marine exhaust gas via in-site combination of ozone oxidation and wet scrubbing absorption, J. Mar. Sci. Eng. 8 (11) (2020) 943, https://doi.org/10.3390/jmse8110943.
[9] Y. Kobashi, Y. Wang, G. Shibata, H. Ogawa, K. Naganuma, Ignition control in a gasoline compression ignition engine with ozone addition combined with a two-stage direct-injection strategy, Fuel 249 (Aug. 2019) 154–160, https://doi.org/10.1016/j.fuel.2019.03.101.
[10] M.R. Khani, E.B. Pour, S. Rashnoo, X. Tu, B. Ghobadian, B. Shokri, A. Khadem, S.I. Hosseini, Real diesel engine exhaust emission control: indirect non-thermal plasma and comparison to direct plasma for NOX, THC, CO, and CO2, Journal of Environmental Health Science and Engineering 18 (2) (Jun. 2020) 743–754, https://doi.org/10.1007/s40201-020-00500-0.
[11] K. Zhu, Y. Cai, Y. Shi, Y. Lu, Y. Zhou, Y. He, The effect of nonthermal plasma on the oxidation and removal of particulate matter under different diesel engine loads, Plasma Process. Polym. 19 (1) (Oct. 2021), 2100104, https://doi.org/10.1002/ppap.202100104.
[12] A. Madhukar, B.S. Rajanikanth, Augmenting NOx reduction in diesel exhaust by combined plasma/ozone injection technique: a laboratory investigation, High Volt. 3 (1) (2018) 60–66, https://doi.org/10.1049/hve.2017.0153.
[13] L. Gu, Y. Cai, Y. Shi, J. Wang, X. Pu, H. Xu, Y. Cui, Experimental study on purification of diesel particulate matter by non-thermal plasma technology, Plasma Chem. Plasma Process. 37 (4) (2017) 1193–1209, https://doi.org/10.1007/s11090-017-9815-9.
[14] J. Zhu, Y. Chen, J. Shang, T. Zhu, Effects of air/fuel ratio and ozone aging on physicochemical properties and oxidative potential of soot particles, Chemosphere 220 (Apr. 2019) 883–891, https://doi.org/10.1016/j.chemosphere.2018.12.107.
[15] M. Apeksha, B.S. Rajanikanth, Plasma/adsorbent system for NOx treatment in diesel exhaust: a case study on solid industrial wastes, Int. J. Environ. Sci. Technol. 16 (7) (May 2018) 2973–2988, https://doi.org/10.1007/s13762-018-1776-x.
[16] M.N. Insani, A. Hayat, N. Amaliyah, A.E.E. Putra, Plasma-ozone treatment of air supply on performance and emissions of diesel engine, IOP Conf. Ser. Earth Environ. Sci. 927 (1) (Dec. 2021), 012026, https://doi.org/10.1088/1755-1315/927/1/012026.
[17] M. Alipour, M.B. Ehghaghi, M. Mirsalim, F. Ranjbar, Energy and exergy analysis of the dual-fuel RCCI engine by ozone-assisted combustion of a lean mixture, J. Therm. Anal. Calorim. 143 (5) (Jan. 2020) 3677–3686, https://doi.org/10.1007/s10973-020-09261-2.
[18] C. Gong, J. Yu, K. Wang, J. Liu, W. Huang, X. Si, F. Wei, F. Liu, Y. Han, Numerical study of plasma produced ozone assisted combustion in a direct injection spark ignition methanol engine, Energy 153 (Jun. 2018) 1028–1037, https://doi.org/10.1016/j.energy.2018.04.096.
[19] A. Madhukar, B.S. Rajanikanth, Cascaded plasma–ozone injection system: a novel approach for controlling total hydrocarbon emission in diesel exhaust, Plasma Chem. Plasma Process. 39 (4) (Feb. 2019) 845–862, https://doi.org/10.1007/s11090-019-09959-8.
[20] R. Fan, Y. Cai, Y. Shi, Y. Cui, Effect of the reaction temperature on the removal of diesel particulate matter by ozone injection, Plasma Chem. Plasma Process. 39 (1) (2018) 143–163, https://doi.org/10.1007/s11090-018-9947-6.
[21] J. Gao, C. Ma, S. Xing, L. Sun, L. Huang, Nanostructure analysis of particulate matter emitted from a diesel engine equipped with a NTP reactor, Fuel 192 (2017) 35–44, https://doi.org/10.1016/j.fuel.2016.12.004.
[22] J. Gao, C. Ma, S. Xing, L. Sun, Oxidation behaviours of particulate matter emitted by a diesel engine equipped with a NTP device, Appl. Therm. Eng. 119 (Jun. 2017) 593–602, https://doi.org/10.1016/j.applthermaleng.2017.03.101.
[23] P. Wang, W. Gu, L. Lei, Y. Cai, Z. Li, Micro-structural and components evolution mechanism of particular matter from diesel engines with non-thermal plasma technology, Appl. Therm. Eng. 91 (Dec. 2015) 1–10, https://doi.org/10.1016/j.applthermaleng.2015.08.010.
[24] M. Babaie, P. Davari, P. Talebizadeh, F. Zare, H. Rahimzadeh, Z. Ristovski, R. Brown, Performance evaluation of non-thermal plasma on particulate matter, ozone and CO2 correlation for diesel exhaust emission reduction, Chem. Eng. J. 276 (Sep. 2015) 240–248, https://doi.org/10.1016/j.cej.2015.04.086.
[25] A.S. Ayodhya, K.G. Narayanappa, An Overview of After-Treatment Systems for Diesel Engines, Environmental Science and Pollution Research, 2018, https://doi.org/10.1007/s11356-018-3487-8.
[26] S. Liebsch, M. Leesch, P. Zumpf, J. Jacob, R. Mehnert, P. Martin, M. Kneisel, EGR cooler fouling reduction: a new method for assessment in early engine development phase, SAE Technical Paper Series (2022), https://doi.org/10.4271/2022-01-0589.
[27] Y. Shi, Y. He, Y. Cai, Z. Li, W. Wang, Y. Zhou, Y. Lu, Y. Yang, Effect of nonthermal plasma with different ozone concentrations on the oxidation and removal of different components in particulate matter, J. Energy Inst. 102 (Jun. 2022) 268–277, https://doi.org/10.1016/j.joei.2022.03.014.
[28] Y. Shi, Y. Lu, Y. Cai, Y. He, Y. Zhou, J. Fang, Evolution of particulate matter deposited in the DPF channel during low-temperature regeneration by non-thermal plasma, Fuel 318 (Jun. 2022), 123552, https://doi.org/10.1016/j.fuel.2022.123552.
[29] Y. Shi, Y. Zhou, Z. Li, Y. Cai, X. Li, Y. He, J. Fang, Effect of temperature control conditions on DPF regeneration by nonthermal plasma, Chemosphere 302 (Sep. 2022), 134787, https://doi.org/10.1016/j.chemosphere.2022.134787.
[30] X. Pu, Y. Cai, Y. Shi, J. Wang, L. Gu, J. Tian, W. Li, Diesel particulate filter (DPF) regeneration using non-thermal plasma induced by dielectric barrier discharge, J. Energy Inst. 91 (5) (Oct. 2018) 655–667, https://doi.org/10.1016/j.joei.2017.06.004.
[31] T. Kuwahara, S. Nishii, T. Kuroki, M. Okubo, Complete regeneration characteristics of diesel particulate filter using ozone injection, Appl. Energy 111 (Nov. 2013) 652–656, https://doi.org/10.1016/j.apenergy.2013.05.041.
[32] X. Li, W. Li, Y. Cai, Y. Shi, Y. Zheng, H. Xu, X. Pu, L. Gu, Deposit removal in EGR cooler and effectiveness improvement by non-thermal plasma reactor with different gas sources, Appl. Therm. Eng. 111 (Jan. 2017) 694–702, https://doi.org/10.1016/j.applthermaleng.2016.09.055.
[33] Y. Shi, Y. Zheng, Y. Cai, W. Li, H. Xu, Experimental study of EGR cooler regeneration aided by oxygen-fed NTP and air-fed NTP, Int. J. Automot. Technol. 17 (3) (2016) 369–376, https://doi.org/10.1007/s12239-016-0038-5.

[34] Y.Y. Chen, Y.X. Cai, X.H. Li, Y.X. Shi, Y. Zheng, Experimental study on regenerating fouled EGR cooler by NTPI technology, Int. J. Automot. Technol. 16 (2) (2015) 183–191, https://doi.org/10.1007/s12239-015-0020-7.

[35] C. Paz, E. Suárez, J. Vence, A. Cabarcos, Fouling evolution on ribbed surfaces under EGR dry soot conditions: experimental measurements and 3D model validation, Int. J. Therm. Sci. 151 (May 2020), 106271, https://doi.org/10.1016/j.ijthermalsci.2020.106271.

[36] C. Paz, E. Suárez, J. Vence, J. Hoard, Evolution of EGR cooler deposits under hydrocarbon condensation: analysis of local thickness, roughness, and fouling layer density, Int. J. Therm. Sci. 161 (Mar. 2021), 106744, https://doi.org/10.1016/j.ijthermalsci.2020.106744.

[37] A. Cabarcos, C. Paz, R. Pérez-Orozco, J. Vence, An image-processing algorithm for morphological characterisation of soot agglomerates from TEM micrographs: development and functional description, Powder Technol. 401 (Mar. 2022), 117275, https://doi.org/10.1016/j.powtec.2022.117275.

[38] M. Matsumo, M. Oguma, M. Toba, K. Tsuchiya, K. Hiroki, T. Kikuchi, K. Tanaka, M. Konno, Investigationof EGR deposit generation mechanism in diesel engine – considering the overallpicture of deposit generating mechanism, Trans. Soc. Automot. Eng. Jpn. Inc 48 (5) (2017) 993–999, https://doi.org/10.11351/jsaeronbun.48.993.

[39] C. Paz, M. Concheiro, M. Conde, S. Díaz, Design of a test bench to evaluate the effect of the application of ozone to the oxidation of soot fouling samples, in: International Conference on Environment Pollution and Prevention, ICEPP-23), 2023.

[40] J. Merkisz, P. Bielaczyc, J. Pielecha, J. Woodburn, RDE testing of passenger cars: the effect of the cold start on the emissions results, in: SAE Technical Paper Series, 2019, https://doi.org/10.4271/2019-01-0747.

[41] C. Paz, E. Suarez, M. Concheiro, J. Vence, Experimental analysis of soot particle fouling on EGR heat exchangers: effect of velocity on the deposited particle size distribution, in: 12th International Conference on Heat Exchanger Fouling and Cleaning, 2017.

[42] C. Paz, M. Concheiro, J. Vence, A. Cabarcos, Experimental study of the effect of hydrocarbon condensation on the fouling deposits of exhaust gas recirculation coolers, in: 13th International Conference on Heat Exchanger Fouling and Cleaning, 2019.

[43] S.R. Yadhuraj, G.S. Babu, M.U. Kumari, Measurement of thickness and roughness using gwyddion, in: 2016 3rd International Conference on Advanced Computing and Communication Systems, ICACCS), 2016, https://doi.org/10.1109/icaccs.2016.7586314.

[44] A.O. Djekoune, K. Messaoudi, K. Amara, Incremental circle hough transform: an improved method for circle detection, Optik 133 (Mar. 2017) 17–31, https://doi.org/10.1016/j.ijleo.2016.12.064.

[45] M.J. Lance, S. Sluder, S. Lewis, J. Storey, Characterization of field-aged EGR cooler deposits, SAE International Journal of Engines 3 (2) (Oct. 2010) 126–136, https://doi.org/10.4271/2010-01-2091.

[46] X. Wang, Y. Wang, F. Guo, D. Wang, Y. Bai, Physicochemical characteristics of particulate matter emitted by diesel blending with various aromatics, Fuel 275 (Sep. 2020), 117928, https://doi.org/10.1016/j.fuel.2020.117928.

[47] N.N. Mustafi, R.R. Raine, B. James, Characterization of exhaust particulates from a dual fuel engine by TGA, XPS, and Raman techniques, Aerosol. Sci. Technol. 44 (11) (Sep. 2010) 954–963, https://doi.org/10.1080/02786826.2010.503668.

[48] T. Batakliev, V. Georgiev, M. Anachkov, S. Rakovsky, S. Rakovsky, Ozone decomposition, Interdiscipl. Toxicol. 7 (2) (2014) 47–59, https://doi.org/10.2478/intox-2014-0008.

[49] K. Hong, J. Park, K. Lee, Experimental evaluation of SOF effects on EGR cooler fouling under various flow conditions, Int. J. Automot. Technol. 12 (6) (2011) 813–820, https://doi.org/10.1007/s12239-011-0093-x.

[50] T. Bera, N. Broom, S. Cook, S. Mulqueen, J. Reid, J. Rimmer, A. Ross, R. Williams, K. Woodall, Thermogravimetric analysis applied to characterisation of the evolution of EGR deposits in a working engine, Int. J. Engine Res. (2022), 146808742211122, https://doi.org/10.1177/14680874221112273.

[51] M. Okubo, N. Arita, T. Kuroki, K. Yoshida, T. Yamamoto, Total diesel emission control technology using ozone injection and plasma desorption, Plasma Chem. Plasma Process. 28 (2) (Jan. 2008) 173–187, https://doi.org/10.1007/s11090-008-9121-7.

[52] R. Atkinson, J. Arey, Atmospheric degradation of volatile organic compounds, Chem. Rev. 103 (12) (Oct. 2003) 4605–4638, https://doi.org/10.1021/cr0206420.

[53] Q. Li, J. Shang, T. Zhu, Physicochemical characteristics and toxic effects of ozone-oxidized black carbon particles, Atmos. Environ. 81 (Dec. 2013) 68–75, https://doi.org/10.1016/j.atmosenv.2013.08.043.

[54] H.M. Daly, A.B. Horn, Heterogeneous chemistry of toluene, kerosene and diesel soots, Phys. Chem. Chem. Phys. 11 (7) (2009) 1069, https://doi.org/10.1039/b815400g.

[55] Y. Liu, C. Liu, J. Ma, Q. Ma, H. He, Structural and hygroscopic changes of soot during heterogeneous reaction with O3, Phys. Chem. Chem. Phys. 12 (36) (2010), 10896, https://doi.org/10.1039/c0cp00402b.

[56] A.R. Chughtai, M.E. Brooks, D.M. Smith, Hydration of black carbon, J. Geophys. Res. Atmos. 101 (D14) (Aug. 1996) 19505–19514, https://doi.org/10.1029/95jd01882.

[57] Y. Bedjanian, M.L. Nguyen, Kinetics of the reactions of soot surface-bound polycyclic aromatic hydrocarbons with O3, Chemosphere 79 (4) (2010) 387–393, https://doi.org/10.1016/j.chemosphere.2010.02.009.

[58] U. Pöschl, T. Letzel, C. Schauer, R. Niessner, Interaction of ozone and water vapor with spark discharge soot aerosol particles coated with benzo[a]pyrene: O3 and H2O adsorption, benzo[a]pyrene degradation, and atmospheric implications, J. Phys. Chem. 105 (16) (Mar. 2001) 4029–4041, https://doi.org/10.1021/jp004137n.

[59] J.S. Lee, T.U. Park, K.-Y. Lee, D.-W. Lee, Enhancement of combustive removal of soot at low temperatures (150°C) using ozone as an oxidant and potassium-substituted lanthanum manganite as a catalyst, Ozone: Science &ampmathsemicolon Engineering 43 (5) (Nov. 2020) 461–475, https://doi.org/10.1080/01919512.2020.1839378.

[60] A.R. Chughtai, G.R. Williams, M.M.O. Atteya, N.J. Miller, D.M. Smith, Carbonaceous particle hydration, Atmos. Environ. 33 (17) (Aug. 1999) 2679–2687, https://doi.org/10.1016/s1352-2310(98)00329-x.

[61] A.R. Chughtai, N.J. Miller, D.M. Smith, J.R. Pitts, Carbonaceous particle hydration III, J. Atmos. Chem. 34 (2) (1999) 259–279, https://doi.org/10.1023/a:1006221326060.

[62] Y. Itoh, Y. Sakakibara, H. Shinjoh, Low-temperature oxidation of particulate matter using ozone, RSC Adv. 4 (37) (2014) 19144–19149, https://doi.org/10.1039/c4ra01003e.

[63] F. Friebel, A.A. Mensah, Ozone concentration versus temperature: atmospheric aging of soot particles, Langmuir 35 (45) (Sep. 2019) 14437–14450, https://doi.org/10.1021/acs.langmuir.9b02372.

[64] A.R. Chughtai, J.M. Kim, D.M. Smith, The effect of temperature and humidity on the reaction of ozone with combustion soot: implications for reactivity near the tropopause, J. Atmos. Chem. 45 (3) (2003) 231–243, https://doi.org/10.1023/a:1024250505886.

[65] M. Knauer, M.E. Schuster, D. Su, R. Schlögl, R. Niessner, N.P. Ivleva, Soot structure and reactivity analysis by Raman microspectroscopy, temperature-programmed oxidation, and high-resolution transmission electron microscopy, J. Phys. Chem. 113 (50) (Nov. 2009) 13871–13880, https://doi.org/10.1021/jp905639d.

[66] J. Gao, C. Ma, S. Xing, L. Sun, L. Huang, A review of fundamental factors affecting diesel PM oxidation behaviors, Sci. China Technol. Sci. 61 (3) (2017) 330–345, https://doi.org/10.1007/s11431-016-9117-x.

[67] X. He, S. Pang, J. Ma, Y. Zhang, Influence of relative humidity on heterogeneous reactions of O3 and O3/SO2 with soot particles: potential for environmental and health effects, Atmos. Environ. 165 (Sep. 2017) 198–206, https://doi.org/10.1016/j.atmosenv.2017.06.049.

[68] A. Liati, P.D. Eggenschwiler, D. Schreiber, V. Zelenay, M. Ammann, Variations in diesel soot reactivity along the exhaust after-treatment system, based on the morphology and nanostructure of primary soot particles, Combust. Flame 160 (3) (Mar. 2013) 671–681, https://doi.org/10.1016/j.combustflame.2012.10.024.

[69] J. Wei, Y. Wang, Effects of biodiesels on the physicochemical properties and oxidative reactivity of diesel particulates: a review, Sci. Total Environ. 788 (Sep. 2021), 147753, https://doi.org/10.1016/j.scitotenv.2021.147753.

[70] K.S. Hong, K.S. Lee, S. Song, K.M. Chun, D. Chung, S. Min, Parametric study on particle size and SOF effects on EGR cooler fouling, Atmos. Environ. 45 (32) (Oct. 2011) 5677–5683, https://doi.org/10.1016/j.atmosenv.2011.07.036.
[71] C. Ma, J. Gao, L. Zhong, S. Xing, Experimental investigation of the oxidation behaviour and thermal kinetics of diesel particulate matter with non-thermal plasma, Appl. Therm. Eng. 99 (Apr. 2016) 1110–1118, https://doi.org/10.1016/j.applthermaleng.2016.01.165.
[72] X. He, C. Leng, S. Pang, Y. Zhang, Kinetics study of heterogeneous reactions of ozone with unsaturated fatty acid single droplets using micro-FTIR spectroscopy, RSC Adv. 7 (6) (2017) 3204–3213, https://doi.org/10.1039/c6ra25255a.